SPACE ENVIRONMENT TECHNOLOGIES

Solar and Geomagnetic Indices for the JB2008 Thermosphere Density Model

W. Kent Tobiska
Bruce R. Bowman
S. Dave Bouwer

August 2008

SOLAR AND GEOMAGNETIC INDICES
FOR THE JB2008 THERMOSPHERE DENSITY MODEL

W. Kent Tobiska, Space Environment Technologies,
ktobiska@spacenvironment.net

Bruce R. Bowman, Air Force Space Command, Space Analysis/A9AC, bruce.bowman@peterson.af.mil

and

S. Dave Bouwer, Space Environment Technologies,
dbouwer@spacenvironment.net

Abstract

Solar and geomagnetic indices are described for use in the Jacchia-Bowman 2008 thermospheric density model (JB2008). There are four solar and two geomagnetic indices used by JB2008. The $F_{10.7}$, $S_{10.7}$, $M_{10.7}$, and $Y_{10.7}$ solar indices are formed using the JB2006 methodology and they map energy from specific solar irradiance sources to major thermospheric layers. Energy that is deposited to the lower thermosphere and mesopause (85-100 km) is now provided. These solar proxies and indices are compliant with the ISO International Standard 21348 for determining solar irradiances. Reference values of the solar indices and proxies for short-term, intermediate-term, solar cycle, and 25-year periods from solar cycle 23 examples are provided for users who want reference values for planning and tests. The a_p geomagnetic and Dst ring current indices are used in a two-index formulation that captures both low/unsettled activity and substorms/storms to represent changes to the neutral thermospheric densities as a result of high-latitude Joule heating and charged particle precipitation. The storm effects change the rate of exospheric temperature change, dTc, which affects satellite orbits. Reference values for a_p, Dst, and dTc are provided using an example storm of November 20-21, 2003 for users who want reference values for planning and tests. Use of these solar, geomagnetic, and ring current indices in the JB2008 model produces significant improvements in empirical thermospheric density modeling. JB2008 provides standard deviations of approximately 9–10% at 400 km, which is a significant decrease from 16% previously obtained using the Jacchia 70 model.

Keywords: JB2008 thermospheric density model, solar indices and proxies, geomagnetic and ring current indices

JB2008 atmospheric density model

The Jacchia-Bowman 2008 thermospheric density model (JB2008) was developed to improve the specification of thermospheric mass densities (Bowman *et al.,* 2008a, Bowman *et al.,* 2008b). The densities are used in LEO satellite orbit determination algorithms to provide a solution for atmospheric drag. The JB2008 empirical atmospheric density model revises and improves the earlier Jacchia-Bowman 2006 (JB2006) model in four ways. First, a new solar index is provided that represents the combined energy input from solar Lyman-α (121 ≤ λ < 122 nm), which is a chromospheric/transition region emission, plus hot coronal X-rays (0.1 ≤ λ < 0.8 nm), both

of which penetrate to the lower thermosphere and mesopause (~85–100 km). Second, new exospheric temperature equations have been developed to characterize the soft X-ray (XUV, $0.1 \le \lambda < 10$ nm), extreme ultraviolet (EUV, $10 \le \lambda < 121$ nm), Lyman-α, and far ultraviolet (FUV, $122 \le \lambda < 200$ nm) thermospheric heating. Third, new equations, based on 81-day averages of multiple solar indices, have been created to model the semiannual density variations. Fourth, geomagnetic storms and substorms are modeled using the 1-hour Dst index while non-storm, but unsettled conditions continue to be modeled using the 3-hour a_p geomagnetic index.

JB2008 was validated through a comparison of its results with very accurate daily drag data at the 2–4% error level. These were computed for numerous satellites as described by Bowman *et al.* (2008b). The satellites' altitude range of 175 to 1000 km also covered a broad range of orbital inclinations as well as solar and geomagnetic conditions from 1997–2007, i.e., inclusive of solar cycle maximum to minimum variations, flare periods, and major as well as minor geomagnetic storm events. Accelerometer measurements during storm conditions from the CHAMP and GRACE satellites were included in the comparisons. The JB2008 model source code, publication list, author contact information, and historical as well as continuously updating real-time and forecast solar and geomagnetic indices are located on the Space Environment Technologies (SET) website https://spacewx.com Mission link leading to the https://spacewx.com/satellite-protection/ menu link.

Solar indices

There are four solar and two geomagnetic indices used by JB2008. The $F_{10.7}$, $S_{10.7}$, $M_{10.7}$, and $Y_{10.7}$ solar indices were created to map energy from specific solar irradiance sources to major thermospheric layers that are dominated by unique atmospheric neutral constituents. The a_p geomagnetic and Dst ring current indices are used to represent changes to the neutral thermospheric densities as a result of high-latitude Joule heating and charged particle precipitation. These processes interact with the dynamics of, and the photoabsorption energy processes in, the neutral atmosphere and lead to increased densities during geomagnetic storms.

The solar indices' formation followed the methodology used for JB2006, which represented a significant departure from solar energy representation in previous Jacchia and MSIS-type empirical models. In the earlier thermosphere models, the solar energy driver evolved from a relationship described by Jacchia (1965, 1971). He used observations that satellite orbit perturbations were highly correlated with the 10.7-cm solar radio flux, $F_{10.7}$. Wolfgang Priester discovered (Priester, 1959) that thermospheric density was correlated with the 20-cm solar emission. In 1960, Hans-Karl Paetzold discovered (Paetzold, 1960) that the correlation failed in the summer because of moisture condensing in the 20-cm antenna, which was in East Berlin. However, Paetzold pointed out that the 10-cm antenna in Ottawa did not have this moisture problem. Using the data from Covington's 10-cm antenna, Paetzold was able to discover the annual and semiannual variations in density. Since that powerful confirmation of the value of the 10-cm solar flux, $F_{10.7}$, aeronomers have customarily used the 10-cm measurements as a proxy for the solar ultraviolet emissions.

$F_{10.7}$ was used by Jacchia to represent all solar energy available for thermospheric heating. Although thermospheric heating is dominated by the solar chromospheric

EUV energy, it also comes from coronal soft X-ray, Lyman-α, and photospheric FUV wavelengths (Banks and Kockarts, 1973). It was the ability to insert more physics into thermospheric density drivers in the form of specific solar wavelengths linked to optical depths that enabled JB2006 to substantially reduce thermospheric densities variation uncertainties (Tobiska *et al.,* 2008; Bowman *et al.,* 2008c, Marcos *et al.,* 2006).

The use of several indices to represent multiple thermospheric heating processes followed an idea first developed by Schmidtke (1976) and extended by Tobiska (1988). In the JB2006 development it was recognized that different solar atmosphere temperature regions and features create specific irradiance wavelengths. These photons arrive at Earth and map to different levels of unit optical depth in the thermosphere, i.e., the level at which most of the photon absorption has occurred. The wavelength-dependent optical depths are defined by species' concentrations convolved with their absorption cross sections integrated by altitude step. In JB2006 three separate solar indices were derived to represent this complex mapping of solar irradiance sources to thermospheric optical depths. JB2008 further extended this methodology to include an additional solar temperature region (the hot corona) and an additional thermospheric layer, i.e., the 85-100 km mesopause and lower thermosphere.

We describe the development and use of the four JB2008 solar indices. The first three indices, $F_{10.7}$, $S_{10.7}$, $M_{10.7}$, were previously discussed (Tobiska *et al.*, 2008) and are recalled here for an expanded, complete treatment. The fourth index, $Y_{10.7}$, is a new index, is similar to the $XL_{10.7}$ from the 2006 discussion, and is fully described here.

$F_{10.7}$ proxy

$F_{10.7}$ was first measured by Covington (1948) on a daily basis beginning February 14, 1947. At the present time the 10.7-cm solar radio flux is measured at the Dominion Radio Astrophysical Observatory (DRAO) in Penticton, British Columbia by the Solar Radio Monitoring Programme, which is operated jointly by the National Research Council (http://www.nrc-cnrc.gc.ca) and the Canadian Space Agency. Observations of the $F_{10.7}$ flux density values are made at 17, 20 and 23 UTC each day then processed and transmitted to users automatically through the DRAO website cimbarop@drao.nrc.ca. The 20 UTC observed values (not 1 AU) are archived at the World Data Center and used for the JB2008 inputs. The physical units of $F_{10.7}$ are $\times 10^{-22}$ W m^{-2} Hz^{-1} and their numerical value is customarily used without the multiplier and called solar flux units (sfu). In other words, a 10.7-cm solar radio emission of 150×10^{-22} W m^{-2} Hz^{-1} is simply referred to as $F_{10.7}$ = 150 sfu.

$F_{10.7}$ is a useful proxy for the combination of chromospheric, transition region, and coronal solar EUV emissions modulated by bright solar active regions whose energies at Earth are deposited in the thermosphere. Because of the high EUV– $F_{10.7}$ correlation, Jacchia developed empirical equations for exospheric temperatures that varied with solar activity and that could be used in atmospheric density models, e.g., CIRA72 (COSPAR, 1972). $F_{10.7}$ does not actually interact with the Earth's (or other planetary) atmospheres, i.e., the radiation can be measured all the way to the Earth's surface. It originates mostly in the solar cool (low) corona by electrons in thermal free-free (bremsstrahlung) emission in the vicinity of sunspots and in widely distributed areas associated with the hot complexes of solar activity (Tapping and DeTracey, 1990).

The dependence on few processes, combined with it localized formation in the cool corona, i.e., a region that is closely coupled with magnetic structures responsible for creating the XUV–EUV irradiances, makes this a good generalized solar proxy for thermospheric heating.

The running 81-day centered smoothed $F_{10.7}$ values, using the moving boxcar method, are referred to as F_{81}. The observed archival daily $F_{10.7}$ values and their 81-day running center-smoothed values, F_{81}, with a 1-day lag are used as described in other work (Bowman, *et al.,* 2008a; Bowman, *et al.,* 2008c). The 1-day lag had the best correlation with satellite-derived density residuals. Figure 1 shows the solar cycle 23 $F_{10.7}$ index from January 1, 1997 to January 1, 2009.

We have used linear regression with daily $F_{10.7}$ to scale and report all other JB2006 and JB2008 solar indices in units of sfu. Days where there are missing data values are not included in the regressions. $F_{10.7}$ is the recognized historical EUV proxy and, by reporting other proxies or indices in sfu, it is very easy to qualitatively identify similarities and differences between them. For solar energy inputs, it is desirable to have solar indices

Fig. 1. $F_{10.7}$ daily and 81-day smoothed values for use by the JB2008 model from January 1, 1997 to January 1, 2009.

and proxies that vary differently through time. This strategy of using multiple solar indices has significantly improved the accuracy of density modeling as reported by Bowman, *et al.* (2008a).
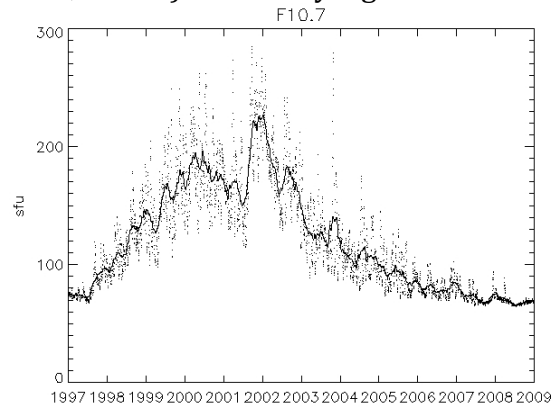
$S_{10.7}$ index

As described by Tobiska *et al.* (2008) the $S_{10.7}$ index is the integrated 26–34 nm solar irradiance that is measured by the Solar Extreme-ultraviolet Monitor (SEM) instrument on the NASA/ESA Solar and Heliospheric Observatory (SOHO) research satellite. SOHO has an uninterrupted view of the Sun by operating in a halo orbit at the Lagrange Point 1 (L1) on the Earth-Sun line, approximately 1.5 million km from the Earth. SEM was built and is operated by University of Southern California's (USC) Space Science Center (SSC) PI team (Judge *et al.,* 2001). SET provides an operational backup system called APEX for the SEM data processing as well as creates and distributes the $S_{10.7}$. SOHO was launched on December 2, 1995 and SEM has been making observations since December 16, 1995. The SEM instrument measures the 26–34 nm solar EUV emission with 15-second time resolution in this first order broadband wavelength range.

The $S_{10.7}$ index is an activity indicator of the integrated 26–34 nm solar emission and is created by first normalizing the data, then converting it to sfu via a first-degree polynomial fit with $F_{10.7}$. Spikes from abnormal flares and missing data were excluded from the fitting vectors. Normalization is achieved for the 1 AU adjusted epoch values, denoted as SOHO_SEM$_{26\_34}$, by division of a mean value over a time frame common to multiple datasets. The mean value = 1.9955×10^{10} photons cm^{-2} s^{-1}. The common time

frame is December 16, 1995 to June 12, 2005, which is generally equivalent to solar cycle 23. The resulting index is called $S_{10.7}$.

In addition to this basic derivation, corrections to $S_{10.7}$ are made as follows. The originally released version of $S_{10.7}$ (v1.8) ranged from January 1, 1996 to December 30, 2005. In versions 3.0–3.9 used by JB2006, the $S_{10.7}$ values between those dates are the original ones derived in v1.8. However, in versions 3.0–3.9 after June 12, 2005, a slight long-term trend was removed to ensure that similar values at the minima of solar cycles 22 and 23 were achieved. For JB2008, ($S_{10.7}$ values v4.0 and higher) a new derivation was completed as given in equation 1 and there may be slight differences of <0.5% compared to earlier versions of $S_{10.7}$. Figure 2 shows $S_{10.7}$ and the S_{81} (81-day centered smoothed) values (v4.0) for solar cycle 23 from January 1, 1997 to January 1, 2009. Daily updated values are found at the JB2008 menu link on the SET https://spacewx.com website.

$$S_{10.7} = (-2.90193) + (118.512) * (SOHO\_SEM_{26\_34}/1.9955\times10^{10}) \qquad (1)$$

Chromospheric He II at 30.4 nm and coronal Fe XV at 28.4 nm dominate the broadband SEM 26-34 nm irradiances but that bandpass includes contributions from other chromospheric, transition region, and coronal lines. We note that when the SOHO SEM and TIMED SEE 26–34 nm integrated data are compared, there are differences in the time series particularly during active solar conditions. It is possible that the SOHO SEM measurements are slightly contaminated with 2nd order emissions from the coronal 17.1 nm Fe IX line that have not been removed; however, this topic needs further

Fig. 2. $S_{10.7}$ (v4.0) daily and 81-day smoothed values for use by the JB2008 model from January 1, 1997 to January 1, 2009.

investigation. The energy in this bandpass principally comes from solar active regions, plage, and network. Once the photons reach the Earth, they are deposited (absorbed) in the terrestrial thermosphere mostly by atomic oxygen above 200 km. We use the daily $S_{10.7}$ index and it's 81-day running center-smoothed values, S_{81}, with a 1-day lag (the best correlation with satellite density residuals) as described in Bowman, *et al.* (2008a). We infer the 1-day lag is consistent with the average atomic oxygen thermal conduction timescale in the thermosphere above 180 km.
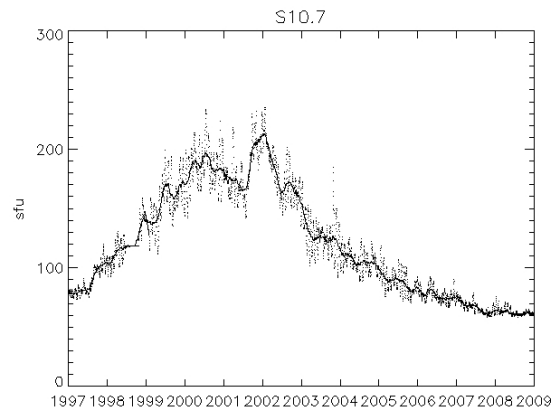
$M_{10.7}$ proxy

Tobiska *et al.* (2006) describe the development of the $M_{10.7}$ index. It is derived from the Mg II core-to-wing ratio that originated from the NOAA series operational satellites, e.g., NOAA-16,-17,-18, which host the Solar Backscatter Ultraviolet (SBUV) spectrometer (Heath and Schlesinger, 1986; Viereck *et al.,* 2001). This instrument has the objective of monitoring ozone in the Earth's lower atmosphere and, secondarily, making solar UV measurements. In its discrete operating mode, a diffuser screen is placed in front of the instrument's aperture in order to scatter solar middle ultraviolet

(MUV) radiation near 280 nm into the instrument. Although the NOAA data are from operational satellites, the SORCE/SOLSTICE and ERS-2/GOME research satellites also make the Mg II cwr measurements.

The 280 nm solar spectral band contains photospheric continuum and chromospheric line emissions. The Mg II *h* and *k* lines at 279.56 and 280.27 nm, respectively, are chromospheric in origin while the weakly varying wings or continuum longward and shortward of the core line emission are photospheric in origin. The instruments from all satellites observe both features. On the ground, the ratio of the Mg II variable core lines to the nearly non-varying wings is calculated. The result is mostly a measure of chromospheric solar active region emission that is theoretically independent of instrument sensitivity change through time. However, long-term changes can occur in the index if instrument wavelength calibrations change in-flight or the solar incidence angle into the instrument changes. The daily Mg II core-to-wing ratio (cwr), described by (Viereck, *et al.,* 2001), has historically been provided through the NOAA Space Weather Prediction Center (SWPC). It is likely, however, that the index values at NOAA SWPC are presently uncorrected. SET has developed and provides a corrected, operational Mg II cwr data product ($MgII_{cwr\_SET}$) available at the Products menu link of https://spacewx.com that uses the NOAA-16,-17-18, SORCE/SOLSTICE, and ERS-2/GOME data sources. Bouwer (2008) describes the detailed processing of the $MgII_{cwr\_SET}$ product. The NOAA data come directly through NOAA NESDIS and SET uses the DeLand algorithm (DeLand and Cebula, 1994; Cebula and DeLand, 1998) to create the index.

The Mg II cwr is an especially good proxy for some solar FUV and EUV emissions. It well represents photospheric and lower chromospheric solar FUV Schumann-Runge Continuum emission near 160 nm that maps into lower thermosphere heating due to O_2 photodissociation (Bowman, *et al.,* 2008a). Since a 160 nm solar FUV emission photosphere index is not produced operationally, the $MgII_{cwr\_SET}$ proxy is used and modified into the $M_{10.7}$ index for comparison with the other solar indices. This derivation is performed in the following manner. A relationship between the long-term (multiple solar cycle) daily $MgII_{cwr\_SET}$ and $F_{10.7}$ is created by making a first-degree polynomial fit to produce a coefficient set that can translate the index into sfu. The result is $M^*_{10.7}$. Next, a correction is added for the decline of solar cycle 23 to account for NOAA 16 instrument degradation that may be related to its diffuser screen illumination geometry changing with time; this cause is unconfirmed. The correction is accomplished by using another first-degree polynomial fit between a trend ratio and day number starting 2448542.0 JD (October 12, 1991 12:00 UT) near the peak of solar cycle 22. The trend ratio is formed from the 365-day center smoothed $M^*_{10.7}$ divided by the 365-day center smoothed $F_{10.7}$. Equation 2 is the final v4.0 formulation of the $M_{10.7}$ index. The derived $M_{10.7}$ index is reported in sfu, i.e., $F_{10.7}$ units with a lower threshold minimum value set to 60. There may be slight differences of up to 1% compared to earlier versions of $M_{10.7}$.

$$M_{10.7} = [-2107.6186 + (8203.0537)*(MgII_{cwr\_SET})] +$$
$$[(M^*_{10.7})*(1.2890589 + (-8.3777235\times10^{-5})*x - 1)] \qquad (2)$$

The day number x = 0, 1, 2, ... with x = 0 equivalent to starting on 2448542.0 JD. Figure 3 shows the $M_{10.7}$ index during solar cycle 23 from January 1, 1997 to January 1, 2009.

The daily $M_{10.7}$ and its 81-day running center-smoothed values, M_{81}, are used with a 2-day lag in JB2008 as a proxy for the Schumann-Runge continuum FUV emission (Bowman, *et al.*, 2008a). Originally, the JB2006 model, which did not use $Y_{10.7}$, had a lag time for $M_{10.7}$ of 5 days since the index was incorporating a combination of lag times from several energy transfer processes in the lower thermosphere to the mesopause. However, with the addition of the lower altitude (85–100 km) relevant $Y_{10.7}$ index, a shorter lag time was appropriate for $M_{10.7}$, which represents O_2 photodissociation, recombination, conduction, and transport processes at the 95–110 km level. We infer the 2-day lag is consistent with the average molecular oxygen dissociation and thermal conduction timescale in the thermosphere above 95 km, although eddy and turbulent conduction processes may play a role.

$Y_{10.7}$ index

The $XL_{10.7}$ index was developed as a candidate index for the JB2006 model (Tobiska *et al.*, 2006) but was unused. While developing the JB2008 model, it was determined that a thermospheric energy contribution to satellite drag from the 80–95 km region was significantly correlated with the composite $XL_{10.7}$ solar index.

Fig. 3. $M_{10.7}$ (v4.0) daily and 81-day smoothed values for use by the JB2008 model from January 1, 1997 to January 1, 2009.

Solar X-rays in the 0.1–0.8 nm wavelength range come from the cool and hot corona and are typically a combination of both very bright solar active region background that varies slowly (days to months) plus flares that vary rapidly (minutes to hours), respectively. The photons arriving at Earth are absorbed in the lower thermosphere to mesopause and (85–100 km) by molecular oxygen (O_2) and molecular nitrogen (N_2) where they ionize those neutral constituents to create the ionospheric D-region.

The X-ray Spectrometer (XRS) instrument is part of the instrument package on the GOES series operational spacecraft. The GOES/XRS provides the historical through current epoch 0.1–0.8 nm solar X-ray emission data with a 1-minute cadence and as low as 5-minute latency. These data, which are particularly useful for flare detection, are continuously reported by NOAA SWPC at their website of http://www.swpc.noaa.gov/.

Tobiska and Bouwer (2005) used the GOES/XRS 0.1–0.8 nm data to develop an index of the solar X-ray active region background, without the flare component, for operational use. This is called the X_{b10} index and is used to represent the daily energy that is deposited into the mesosphere and lower thermosphere.

While the 0.1-0.8 nm X-rays are a major energy source in these atmospheric regions during high solar activity, they relinquish their dominance to another emission that reaches the same optical depth, i.e., the competing hydrogen (H) Lyman-α emission that is the major energy source in this atmosphere region during moderate and low solar activity. Lyman-α is created in the solar upper chromosphere and transition
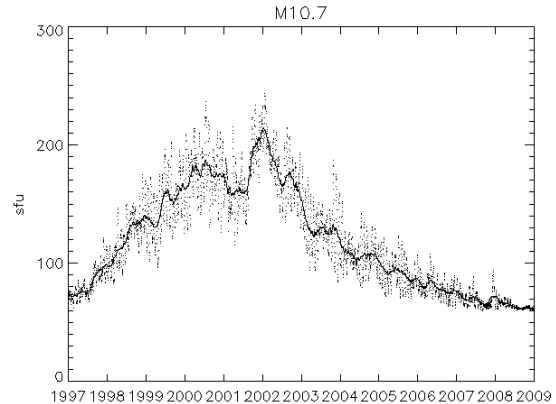
region and demarcates the EUV from the FUV spectral regions. It is formed primarily in solar active regions, plage, and network; the photons, arriving at Earth, are absorbed in the mesosphere and lower thermosphere where they dissociate nitric oxide (NO) and participate in water (H_2O) chemistry. Lyman-α is regularly observed by the SOLSTICE instrument on the UARS and SORCE satellites as well as by the SEE instrument on TIMED (Woods, *et al.,* 2000).

Since these two solar emissions are competing drivers to the mesosphere and lower thermosphere, we have developed a composite solar index of the X_{b10} and Lyman-α. It does not contain a flare component and is weighted to represent mostly X_{b10} during solar maximum and to represent mostly Lyman-α during moderate and low solar activity. A normalized F_{81}, F_{81norm}, consisting of the 81-day centered smoothed $F_{10.7}$ divided by it's mean value for the common time frame of January 1, 1991 through February 16, 2008 is used as the weighting function and multiplied with the X_{b10} and Lyman-α (Lya) expressed as ratios to their solar maximum values. The resulting index is called $Y_{10.7}$ and equations 3, 4, and 5 describe this index as reported in sfu.
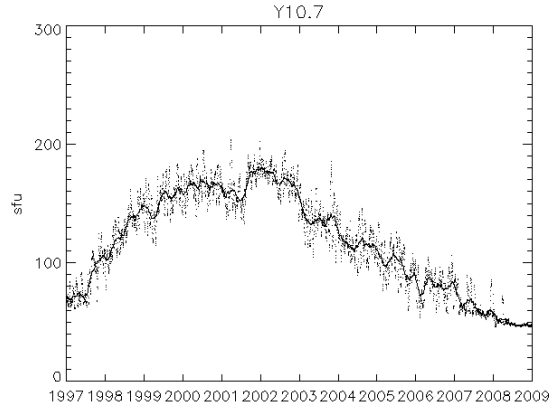
Fig. 4. $Y_{10.7}$ (v4.0) daily and 81-day smoothed values for use by the JB2008 model from January 1, 1997 to January 1, 2009.

$$Y_{10.7} = F_{81norm} * X10 + [(1- F_{81norm}) * L10] \qquad (3)$$

$$L10 = -88.3926 + (3.35891 \times 10^{-10} * Lya) + (2.40481 \times 10^{-22} * Lya^2) \qquad (4)$$

$$X10 = [(-42.5991 + (0.533669 * X_{b10})] \qquad (5)$$

X10 has a minimum threshold value of 40.

This daily index was tested with multi-day lags and the 5-day lag was found to have the strongest correlation signal in the satellite drag density residuals after modeled density variations due to the other solar indices were removed. The 81-day running center-smoothed values, Y_{81}, are also used with the 5-day lag. We infer the 5-day lag is consistent with the average molecular oxygen and molecular nitrogen thermal conduction timescales in the lower thermosphere above 85 km, although eddy and turbulent conduction may also play a role. Figure 4 shows the $Y_{10.7}$ index during solar cycle 23 from January 1, 1997 to January 1, 2009.

Figure 5 provides a comparison between all 4 indices for the time frame of January 1, 1997 to January 1, 2009. The 81-day smoothed values are used to highlight the trends of each proxy or index. Figure 5 shows that each index or proxy captures a different type of solar energy variability. The composite of these 4 indices and proxies is the most complete representation to date, for empirical thermospheric density models, of the solar XUV, EUV, Lyman-α, and FUV energy that is deposited at optical depths ranging from 85 km to above 200 km. It is these energies that heat the thermosphere and affect satellite orbits. By expressing the proxies and indices in common units, their contribution to the daily density variability in the JB2008 exospheric

9

temperature equation for Tc can be determined. The $F_{10.7}$ contribution to Tc daily variability is 9.8%, $S_{10.7}$ is 74.1%, $M_{10.7}$ is 10.3%, and $Y_{10.7}$ is 5.8%.

Table A provides the mapping of each index, including the data used to derive them, from its solar irradiance source(s) to the thermospheric optical depth(s) in which it is effective. The table includes the ISO 21348 spectral category, ISO 21348 spectral sub-category, wavelength range in units of nm, solar source temperature region, solar source feature, altitude region of terrestrial atmosphere absorption at unit optical depth in units of km, and terrestrial atmosphere thermal region of energy absorption. The indices and proxies that are marked with an asterisk (*) have been selected for use in the JB2008 empirical thermospheric density model and specifically in its exospheric temperature equation. Table B summarizes the characteristics of the daily solar indices including their observing facility, the instrument(s) used for observing the index/proxy, the nominal observation time frame, the measurement cadence, latency, and an assessment of the observational availability.
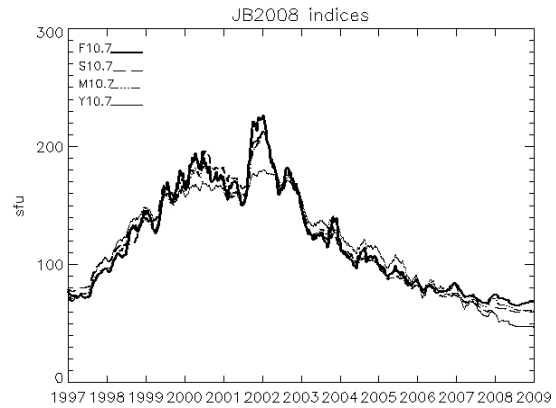
Fig. 5. F_{81}, S_{81}, M_{81}, Y_{81} (v4.0) values for use by the JB2008 model from January 1, 1997 to January 1, 2009.

ISO 21348 compliance

ISO 21348 (2007) defines solar spectral irradiance wavelength ranges as well as solar indices and proxies. Solar irradiance indices and proxies are surrogates for solar irradiances: a solar irradiance proxy is a measured or modeled data type used as a *substitute* for solar spectral irradiances while a solar irradiance index is a measured or modeled data type that is an *indicator* of a solar spectral irradiance activity level. Both can represent line, continua, and integrated irradiances or other irradiance-related solar features such as irradiance deficit from sunspots or sunspot numbers. Solar irradiance proxies and indices are related to solar processes, can be reported over time intervals, and can represent spectral irradiance variations. In this document the four solar proxies and indices are classified as ISO 21348 Type 5 solar irradiance products representing FUV, Lyman-α, EUV, and XUV spectral categories. The processes used for determining solar irradiance indices and proxies reported herein are compliant with ISO International Standard 21348: *Space environment (natural and artificial) – process for determining solar irradiances.*

Reference values

It is useful to have reference values of $F_{10.7}$, $S_{10.7}$, $M_{10.7}$, and $Y_{10.7}$ solar indices for long-term (25 years and solar cycle 23: 1997-2008), intermediate-term (>27 days), and short-term (daily) solar variability conditions. These can be used to test model scenarios under standardized conditions of solar and geomagnetic activity if forecasts are not available.

10

Table A. Solar indices related to atmospheric heating

Index	IS 21348 Spectral category	IS 21348 Spectral sub-category	Wave-length range (nm)	Solar source temperature region[1]	Solar source feature[1]	Atmosphere absorption (unit optical depth, km)[2]	Terrestrial atmosphere absorption (thermal region)[2]
*$F_{10.7}$	Radio	Radio	10.7E7	Transition region, cool corona	Active region	90-500	Thermosphere with 1-day lag; 9.8% daily variability contribution
*$S_{10.7}$	UV	EUV	26-34	Chromosphere, corona	Active region, plage, network	200-300	Thermosphere with 1-day lag; 74.1% daily variability contribution
*$M_{10.7}$	UV	FUV	160	Photosphere-lower chromosphere	SRC	95-110	Lower thermosphere with 2-day lag; 10.3% daily variability contribution
$MgII_{cwr}$	UV	MUV	280[3]	Chromosphere	Active region, plage, network	200-300	Thermosphere
*$Y_{10.7}$	X-rays and UV	X-rays+H Lyman-α	0.1-0.8, 121	Chromosphere, transition region, hot corona	Active region, plage, network	85-100	Mesopause-lower thermosphere with 5-day lag; 5.8% daily variability contribution
H Lya	UV	H Lyman-α	121	Transition region, chromosphere	Active region, plage, network	85-100	Mesopause-lower thermosphere
X_{b10}	X-rays	X-rays	0.1-0.8	Hot corona	Active region background	85-100	Mesopause-lower thermosphere

*Index or proxy is used in the JB2008 model exospheric temperature equation.
[1]Vernazza *et al.,* 1976; Vernazza *et al.,* 1981.
[2]Banks, P. and G. Kockarts, 1973.
[3]The *h* & *k* lines at the band center are chromospheric and are referenced to blackbody continuum wings at edges of bandpass.

Table B. Characteristics of daily JB2008 solar indices

Index or proxy	Observing facility	Instrument	Observation time frame	Measurement cadence	Measurement latency	Operational availability
$F_{10.7}$	Penticton ground observatory	Radio telescope	1947-2009	3 times/day	Up to 24 hours	yes
$S_{10.7}$	SOHO, GOES	SEM, EUVS	1996-2009	15-second	Up to 24 hours	(a)
$M_{10.7}$	NOAA-16,17,18, SORCE, ERS-2	SBUV, SOLSTICE, GOME	1991-2009	2 times/day	Up to 24 hours	yes
$Y_{10.7}$	GOES-12, UARS, SORCE, TIMED	XRS, SOLSTICE (2), SEE	1991-2009	1-minute, 16 times/day	Up to 10 minutes, up to 48 hours	(b)

(a) SOHO/SEM is a NASA research instrument but provides daily irradiances on an operational cadence; GOES 13 EUVS B channel makes measurements in the same bandpass as SOHO SEM.
(b) GOES XRS is a NOAA operational instrument whereas TIMED/SEE and SORCE/SOLSTICE are NASA research instruments providing daily irradiances on an operational measurement cadence.
(c) UARS/SOLSTICE stopped in 2005; SORCE/SOLSTICE intends to provide data for several years.

Intermediate-term and short-term solar variability reference values

Reference index values are provided in Table C for intermediate-term variability that includes more than one solar rotation (>27 days) but for not more than a half solar cycle (<6 years). The 81-day smoothed minimum, mean, and maximum values rounded to the nearest unit of 5 for solar cycle 23 are used for reference low, moderate, and high intermediate-term examples, respectively.

Daily (short-term) solar variability reference values for less than a solar rotation (27 days) are also provided in Table C as rounded numbers to the nearest unit of 5. The period of October 14 to November 9, 2003 in solar cycle 23 is used as a reference period when highly variable activity occurred; these are conditions appropriate to the

rise of a solar cycle or large events that occur during the decline of a solar cycle. A second period is provided from January 7 to February 2, 2005 when lower variable activity occurred; these are conditions appropriate approaching or leaving the minimum of a solar cycle. In short-term periods, higher values have been measured than those given in Table C, e.g., F10.7 = 380 over a day. However, empirical atmosphere density models are not developed for such high index values and their use will lead to large and unknown errors.

In Table C, the example Cases 1, 2, and 3 should use the low, moderate, and high solar activity levels for that Case only as one complete set of inputs into JB2008. The 81-day value should be set to the moderate Case value for each proxy or index. Values from different Case examples should not be mixed. If a single daily value from one Case and one solar activity level is desired, the 81-day index should be set to the moderate value for each index.

Table C. Reference values for intermediate- and short-term solar variability

Daily	Case 1: Intermediate-term (81 days)			Case 2: Short-term (27 days high activity)			Case 3: Short-term (27 days low activity)		
	Low	Moderate	High	Low	Moderate	High	Low	Moderate	High
$F_{10.7}$	65	120	225	90	165	280	80	105	145
$S_{10.7}$	60	120	215	105	135	185	85	100	120
$M_{10.7}$	60	115	215	95	135	185	80	95	115
$Y_{10.7}$	50	115	180	110	150	185	90	110	135

Long-term solar cycle variability

Tables D1 and D2 are provided for estimating solar cycle variability in the four solar indices. The example of solar cycle 23, a moderate cycle, is used. In these tables, the actual monthly minimum, mean, and maximum value of each index or proxy is given. Table D1 reports monthly values for the $F_{10.7}$, F_{81} proxy and the $S_{10.7}$, S_{81} index. Table D2 reports monthly values for the $M_{10.7}$, M_{81} proxy and the $Y_{10.7}$, Y_{81} index.

The ranges of maximum and minimum values are not the confidence values since they are the actual measurements. Smaller solar cycles will tend to produce a smaller monthly range and larger solar cycles will tend to produce a larger monthly range. Solar cycle 23 is considered a moderate cycle by recent historical standards.

The table values should be used as provided for periods of up to a solar cycle if no forecasts are available. If daily values are required, the monthly values can be interpolated to daily resolution. Figure 5 shows all four proxies and indices. Daily forecasts for $F_{10.7}$, F_{81}, $S_{10.7}$, S_{81}, $M_{10.7}$, M_{81}, $Y_{10.7}$, and Y_{81} out to 5 solar rotations (137-days) are provided by Space Environment Technologies upon request at data@spacewx.com.

Table D1. Reference values for long-term solar cycle variability in the $F_{10.7}$, F_{81} proxy and $S_{10.7}$, S_{81} index

Month	$F10_{min}$	$F10_{mean}$	$F10_{max}$	$F81_{min}$	$F81_{mean}$	$F81_{max}$	$S10_{min}$	$S10_{mean}$	$S10_{max}$	$S81_{min}$	$S81_{mean}$	$S81_{max}$
0	72	74	77	74	76	78	74	78	82	78	79	79
1	71	74	81	74	74	74	74	77	82	78	78	78
2	70	73	76	74	74	74	73	78	83	78	79	79

Month	$F10_{min}$	$F10_{mean}$	$F10_{max}$	$F81_{min}$	$F81_{mean}$	$F81_{max}$	$S10_{min}$	$S10_{mean}$	$S10_{max}$	$S81_{min}$	$S81_{mean}$	$S81_{max}$
3	69	74	81	74	74	74	74	80	86	79	80	81
4	71	75	85	72	73	74	78	83	91	81	81	81
5	68	72	77	72	72	73	78	81	87	81	81	82
6	67	71	80	73	74	77	75	80	87	82	83	86
7	71	79	96	78	82	86	80	89	100	86	90	94
8	85	96	119	86	88	91	97	100	103	94	96	99
9	79	85	91	91	92	93	92	98	103	99	100	102
10	86	100	118	93	95	96	97	105	120	102	102	103
11	85	99	117	96	97	97	95	104	114	103	104	105
12	81	93	108	94	95	96	92	104	110	103	104	105
13	83	93	107	95	99	103	93	103	110	104	106	108
14	90	109	133	103	106	108	97	110	123	109	111	113
15	88	108	141	109	110	110	101	117	131	114	115	116
16	87	107	133	106	107	109	103	114	125	116	116	117
17	96	108	122	108	109	111	108	119	128	116	117	117
18	99	114	129	112	119	127	118	118	118	117	118	119
19	109	136	179	127	130	133	118	118	118	118	118	118
20	116	138	177	130	132	133	118	118	118	118	119	122
21	103	117	135	128	130	132	118	120	130	122	125	131
22	115	140	168	132	136	140	123	139	158	131	136	140
23	129	150	184	140	143	147	140	147	159	139	141	142
24	110	141	178	142	145	147	128	136	143	138	139	140
25	99	142	205	135	139	143	115	138	159	137	138	139
26	102	126	156	127	130	135	119	139	154	137	138	139
27	98	117	141	127	130	134	111	132	151	139	141	144
28	127	149	178	134	144	154	130	153	168	145	152	159
29	139	170	210	155	161	167	154	171	192	160	165	170
30	130	166	206	164	166	169	156	172	200	169	170	171
31	123	171	248	155	159	166	146	169	194	161	164	170
32	107	136	163	153	156	159	136	151	184	158	160	162
33	122	165	200	160	165	169	149	159	168	160	162	165
34	143	192	249	169	176	181	157	177	193	165	169	170
35	130	170	217	166	174	178	144	169	192	169	172	173
36	126	158	211	163	167	172	142	167	200	170	171	173
37	138	173	227	172	179	186	155	177	194	174	179	183
38	178	208	234	185	189	192	173	193	213	183	187	189
39	158	184	223	187	191	195	179	192	214	188	189	191
40	127	185	262	181	183	187	165	183	212	184	186	188
41	148	180	202	184	191	196	165	185	206	185	191	195
42	148	202	262	181	185	187	176	207	234	193	196	197
43	131	163	194	174	180	184	162	189	213	187	192	195
44	133	182	232	170	171	173	166	181	197	181	183	187
45	140	168	203	173	176	179	166	183	197	181	182	183
46	144	179	205	171	173	176	157	185	224	182	183	184

Month	$F10_{min}$	$F10_{mean}$	$F10_{max}$	$F81_{min}$	$F81_{mean}$	$F81_{max}$	$S10_{min}$	$S10_{mean}$	$S10_{max}$	$S81_{min}$	$S81_{mean}$	$S81_{max}$
47	135	174	201	172	174	176	156	184	209	182	183	184
48	152	167	184	160	165	172	172	178	185	175	179	183
49	130	147	170	155	161	167	158	170	184	171	174	176
50	130	178	274	165	168	170	155	175	218	174	174	176
51	123	178	258	169	170	172	152	178	215	173	174	174
52	129	148	185	160	165	171	151	165	186	170	172	174
53	133	174	221	150	153	160	162	176	190	165	167	170
54	115	131	150	151	154	158	142	156	168	166	166	167
55	120	163	199	158	173	187	143	168	180	167	173	181
56	183	234	285	188	203	218	174	199	230	182	191	200
57	171	208	248	218	220	222	192	207	222	201	204	206
58	170	213	271	214	220	226	182	201	232	204	206	209
59	206	236	275	223	224	225	197	211	232	207	209	212
60	189	227	261	217	223	227	197	219	235	211	212	213
61	188	205	246	201	206	216	199	205	218	202	206	211
62	166	179	204	186	193	201	181	191	196	191	196	202
63	147	190	226	181	183	186	171	189	203	183	187	191
64	157	178	191	161	172	181	161	180	194	171	177	183
65	131	149	179	159	162	165	150	163	183	164	166	170
66	129	174	242	163	168	175	144	161	181	163	165	167
67	135	184	241	176	181	183	149	172	202	167	170	172
68	138	176	221	174	178	182	153	174	198	170	172	173
69	136	167	183	164	170	174	150	164	180	163	166	170
70	137	169	199	162	165	169	149	162	176	160	163	166
71	114	157	213	148	157	162	135	164	177	154	158	161
72	115	144	189	136	143	148	133	149	172	144	150	154
73	102	125	150	129	133	136	111	135	151	134	138	143
74	89	132	160	126	127	129	102	131	153	126	130	133
75	99	126	158	121	123	126	109	128	149	123	125	126
76	92	116	149	122	124	126	104	123	142	124	125	126
77	106	129	193	125	126	127	107	125	139	125	126	127
78	99	128	157	122	126	128	108	127	134	125	126	126
79	107	122	137	117	119	122	114	124	136	123	124	125
80	94	112	137	115	122	132	106	121	135	122	123	126
81	92	151	279	129	135	141	110	129	185	123	125	127
82	91	141	210	137	138	140	100	128	153	123	124	126
83	86	115	143	121	126	140	92	118	143	117	119	123
84	87	114	135	111	113	120	96	109	126	111	113	117
85	95	107	122	108	110	111	101	109	120	109	111	112
86	90	112	129	105	107	108	101	114	125	109	111	112
87	88	101	117	102	104	105	99	109	117	108	109	110
88	85	100	118	97	99	102	99	104	111	102	105	107
89	82	97	119	97	104	108	93	102	109	102	103	104
90	78	119	175	106	110	112	89	105	125	103	104	105

Month	$F10_{min}$	$F10_{mean}$	$F10_{max}$	$F81_{min}$	$F81_{mean}$	$F81_{max}$	$S10_{min}$	$S10_{mean}$	$S10_{max}$	$S81_{min}$	$S81_{mean}$	$S81_{max}$
91	83	110	149	107	112	115	88	105	118	103	105	106
92	88	103	131	102	105	107	93	103	112	102	103	105
93	87	106	140	106	107	108	92	105	122	104	104	105
94	95	114	141	106	106	107	103	108	113	104	104	104
95	85	95	111	99	103	106	92	97	106	99	101	103
96	83	102	145	97	99	100	86	98	119	95	97	98
97	75	97	122	93	97	99	76	94	109	92	94	95
98	74	90	114	90	91	93	76	88	101	88	90	91
99	77	86	106	91	92	93	81	86	92	88	89	90
100	82	100	126	93	95	99	85	92	100	89	90	91
101	77	94	116	94	96	99	82	89	98	90	91	92
102	71	96	130	91	93	95	76	92	107	89	89	90
103	75	91	111	89	91	95	72	88	103	87	88	90
104	72	91	119	85	86	89	74	87	101	84	85	87
105	72	77	83	83	84	85	70	78	83	80	82	84
106	77	86	102	83	85	86	76	80	84	80	81	82
107	85	91	106	86	87	88	79	86	93	82	83	83
108	77	83	94	81	83	86	76	83	89	80	81	83
109	74	77	79	78	79	80	72	76	79	77	78	80
110	72	75	86	79	80	82	71	74	78	77	78	80
111	76	89	101	82	82	83	78	84	92	79	80	82
112	72	81	93	81	82	83	72	83	92	80	81	82
113	72	77	86	76	78	81	73	76	82	76	78	80
114	70	76	87	76	77	78	70	74	82	74	75	76
115	70	79	89	77	78	79	69	73	79	74	74	75
116	70	78	87	78	78	78	67	75	82	74	74	74
117	70	74	80	78	79	81	66	72	78	74	74	75
118	77	86	97	81	83	84	73	77	81	74	74	75
119	72	84	103	84	84	85	68	75	90	75	75	75
120	76	83	92	79	81	84	72	75	80	73	73	74
121	73	78	90	75	77	79	68	72	77	71	72	73
122	69	72	76	73	74	75	64	69	73	68	69	71
123	68	72	87	73	73	75	63	67	71	68	68	69
124	67	74	87	74	74	75	66	68	71	68	69	69
125	65	74	87	72	73	75	61	70	79	68	68	69
126	66	72	79	70	71	72	62	67	70	65	66	68
127	67	69	72	68	69	70	62	64	66	63	64	65
128	65	67	71	68	68	68	60	61	65	62	62	63
129	66	68	69	68	68	70	59	62	66	61	61	62
130	67	70	72	70	72	74	59	60	63	61	62	63
131	71	79	94	74	75	75	60	65	71	63	64	65
132	70	74	80	72	74	75	60	67	76	64	64	65
133	70	71	73	72	72	72	61	64	67	63	64	64
134	68	73	89	71	72	72	60	64	72	63	63	63

Month	$F10_{min}$	$F10_{mean}$	$F10_{max}$	$F81_{min}$	$F81_{mean}$	$F81_{max}$	$S10_{min}$	$S10_{mean}$	$S10_{max}$	$S81_{min}$	$S81_{mean}$	$S81_{max}$
135	67	70	78	70	71	71	63	66	71	63	63	63
136	66	68	72	67	68	70	60	63	68	62	62	63
137	65	66	67	66	67	67	59	61	63	61	61	62
138	65	66	67	66	66	66	58	61	64	61	61	61
139	65	66	68	66	66	67	59	60	62	60	61	61
140	65	67	69	67	67	68	59	61	63	61	61	61
141	66	68	72	68	68	68	60	63	65	61	62	62
142	67	69	71	69	69	69	60	62	65	61	62	62
143	68	69	71	69	69	69	60	61	63	61	62	62

Table D2. Reference values for long-term solar cycle variability in the $M_{10.7}$, M_{81} proxy and $Y_{10.7}$, Y_{81} index

Month	$M10_{min}$	$M10_{mean}$	$M10_{max}$	$M81_{min}$	$M81_{mean}$	$M81_{max}$	$Y10_{min}$	$Y10_{mean}$	$Y10_{max}$	$Y81_{min}$	$Y81_{mean}$	$Y81_{max}$
0	65	72	76	72	73	74	62	66	73	69	71	74
1	62	71	75	72	72	73	63	70	84	69	69	71
2	66	73	80	73	73	74	61	71	80	71	72	72
3	67	75	86	74	75	76	63	74	87	72	73	74
4	72	78	87	76	76	77	64	76	92	72	73	75
5	70	76	86	76	76	77	65	71	86	72	72	73
6	68	75	85	76	77	80	63	70	91	73	75	80
7	73	82	99	80	84	88	65	85	104	81	87	92
8	81	94	101	88	90	92	96	103	110	92	94	98
9	85	91	98	92	93	95	68	90	100	98	100	102
10	84	98	121	95	96	97	98	112	125	101	103	104
11	84	100	120	97	98	99	91	106	120	104	105	106
12	85	99	114	97	98	99	77	101	114	102	103	104
13	85	96	107	98	99	102	91	102	116	103	106	111
14	83	103	117	103	106	109	102	115	131	111	114	118
15	94	113	147	109	111	112	105	120	136	118	120	121
16	90	110	129	112	113	114	107	122	138	120	121	122
17	99	115	139	115	117	119	113	122	129	122	123	125
18	111	128	150	119	125	130	117	127	137	125	130	134
19	122	135	148	130	132	134	132	142	162	135	136	138
20	121	137	151	132	134	135	130	140	154	138	139	139
21	109	126	137	131	133	135	123	132	138	138	139	141
22	116	137	169	134	136	138	129	148	162	141	143	145
23	126	146	175	137	139	140	142	149	158	145	148	149
24	109	138	166	137	138	140	126	149	171	146	147	148
25	102	134	172	134	135	138	123	144	167	142	144	147
26	109	130	159	130	132	134	117	136	157	137	138	142
27	97	121	157	131	132	135	115	131	143	137	139	141

Month	$M10_{min}$	$M10_{mean}$	$M10_{max}$	$M81_{min}$	$M81_{mean}$	$M81_{max}$	$Y10_{min}$	$Y10_{mean}$	$Y10_{max}$	$Y81_{min}$	$Y81_{mean}$	$Y81_{max}$
28	117	145	175	135	142	150	140	151	172	141	147	152
29	135	163	197	151	156	160	152	159	175	153	156	159
30	132	162	191	159	160	162	140	159	177	158	159	160
31	129	162	202	152	155	161	140	162	181	155	157	159
32	121	142	175	150	152	154	135	147	164	154	155	156
33	131	153	167	153	156	158	144	157	165	156	158	160
34	141	170	195	158	161	164	151	170	184	160	162	163
35	125	159	191	162	165	167	140	158	173	158	161	163
36	129	162	209	163	164	166	138	156	175	157	158	160
37	131	167	193	166	170	174	148	162	174	160	163	166
38	156	185	213	174	178	181	163	173	182	165	166	167
39	164	186	213	178	180	183	153	163	178	165	167	168
40	141	172	210	173	176	179	139	163	188	163	164	165
41	145	174	197	174	181	184	152	164	174	164	168	171
42	156	196	236	181	185	187	152	177	194	167	168	169
43	131	177	220	177	182	183	144	161	176	164	166	168
44	150	173	196	173	174	176	150	164	178	163	163	164
45	153	175	200	173	174	176	153	165	175	164	166	168
46	137	179	211	173	174	176	149	170	183	166	166	167
47	126	174	203	172	174	176	149	164	181	164	165	167
48	148	172	188	165	170	176	154	161	167	156	159	163
49	127	156	179	159	162	165	137	148	162	155	157	160
50	137	158	216	157	159	164	140	166	204	159	160	161
51	116	163	204	158	159	162	144	163	203	161	161	162
52	125	154	173	161	161	163	137	150	167	156	158	161
53	147	171	194	159	161	163	147	162	175	152	153	155
54	133	152	172	159	160	161	133	145	153	153	154	157
55	133	157	182	161	166	173	135	160	177	157	162	167
56	172	194	223	173	184	194	167	181	191	167	172	177
57	176	202	234	194	198	201	162	173	182	175	176	177
58	168	192	207	200	202	206	164	175	191	175	176	179
59	196	212	232	203	207	212	171	182	203	179	179	180
60	195	219	243	211	213	214	173	181	188	179	180	180
61	192	207	230	202	206	211	171	177	185	177	177	179
62	176	188	202	190	195	202	166	174	186	176	177	178
63	167	188	212	185	187	190	166	179	190	176	176	177
64	157	184	210	173	180	185	167	175	182	168	172	176
65	143	167	190	166	169	172	153	161	175	167	167	167
66	139	164	201	165	167	169	150	169	188	166	168	170
67	134	174	214	169	173	175	156	175	195	170	171	172
68	144	177	207	174	175	176	151	166	177	168	170	171
69	145	168	190	165	170	173	152	166	180	164	166	168
70	140	163	185	161	165	169	152	166	181	163	165	167
71	130	164	193	153	159	163	135	162	182	155	160	163

Month	$M10_{min}$	$M10_{mean}$	$M10_{max}$	$M81_{min}$	$M81_{mean}$	$M81_{max}$	$Y10_{min}$	$Y10_{mean}$	$Y10_{max}$	$Y81_{min}$	$Y81_{mean}$	$Y81_{max}$
72	128	149	182	143	149	154	137	151	167	146	151	155
73	109	130	163	132	137	142	116	138	152	138	142	145
74	94	131	172	126	129	132	113	137	154	135	136	138
75	106	130	158	123	125	126	114	136	161	132	133	134
76	94	122	147	124	125	128	105	130	145	133	134	136
77	103	126	151	127	128	131	122	138	163	135	136	137
78	113	134	150	129	130	131	122	138	152	135	137	137
79	118	129	141	126	128	130	131	135	146	132	134	135
80	106	123	145	125	127	130	118	130	142	131	134	138
81	102	133	187	126	129	133	110	144	185	136	138	141
82	92	134	175	128	129	131	113	142	177	138	139	140
83	84	121	159	121	123	128	100	129	151	128	132	138
84	88	112	152	112	115	120	101	123	143	122	124	128
85	91	108	127	109	111	112	106	117	123	118	120	121
86	90	110	126	107	109	110	108	120	130	115	117	118
87	95	108	122	107	108	109	100	113	135	113	115	116
88	95	104	113	101	104	107	101	111	122	109	111	113
89	87	101	116	101	103	105	94	110	123	109	112	114
90	79	106	142	102	105	106	90	118	143	113	116	118
91	83	106	135	105	107	108	96	119	146	117	120	121
92	85	105	131	103	106	108	96	117	136	114	115	117
93	94	108	131	106	107	109	94	111	131	113	115	116
94	99	112	129	107	107	108	107	121	130	113	114	116
95	87	102	116	101	104	107	100	110	122	111	113	115
96	83	98	117	97	99	101	90	110	134	105	108	111
97	74	96	121	94	96	97	76	101	117	100	103	105
98	72	90	113	91	92	94	77	96	118	97	98	99
99	75	88	101	91	92	94	82	95	109	98	100	101
100	92	98	109	93	94	96	93	109	124	101	104	107
101	79	93	107	94	95	97	87	104	116	105	106	108
102	71	95	123	92	93	95	75	106	126	101	103	105
103	72	94	118	90	92	94	79	99	121	97	101	104
104	72	90	105	87	89	91	74	99	115	90	93	98
105	71	81	93	85	86	88	60	77	89	86	88	90
106	76	84	91	84	85	87	81	90	104	86	87	89
107	80	92	107	86	87	87	90	97	108	86	89	91
108	75	86	102	82	85	86	62	82	98	76	81	86
109	72	78	86	79	80	82	53	66	77	72	74	76
110	70	76	81	80	81	83	62	72	88	74	77	82
111	77	88	108	83	84	86	82	91	104	82	84	87
112	69	87	106	84	85	86	74	87	101	85	86	87
113	72	79	87	80	81	84	68	81	91	80	82	86
114	70	79	91	78	78	80	59	78	95	80	80	81
115	67	77	83	77	78	79	63	82	97	79	81	82

Month	$M10_{min}$	$M10_{mean}$	$M10_{max}$	$M81_{min}$	$M81_{mean}$	$M81_{max}$	$Y10_{min}$	$Y10_{mean}$	$Y10_{max}$	$Y81_{min}$	$Y81_{mean}$	$Y81_{max}$
116	66	77	92	75	76	78	66	80	93	77	78	80
117	63	72	83	74	75	76	58	69	84	78	78	79
118	63	77	86	74	75	76	72	87	97	79	81	83
119	62	76	89	76	77	77	61	83	106	80	83	84
120	67	77	88	74	75	76	69	81	90	72	76	80
121	67	74	84	71	73	74	56	64	86	66	69	72
122	64	68	74	69	69	71	59	63	70	62	64	66
123	62	68	80	69	69	71	55	65	89	65	66	68
124	64	70	80	70	71	72	57	69	83	68	69	70
125	62	73	89	71	71	72	55	69	87	65	67	70
126	61	70	76	68	69	71	56	64	81	61	63	65
127	60	66	70	66	67	68	56	59	64	58	59	61
128	60	64	67	65	65	66	54	57	61	56	57	58
129	61	64	67	65	65	67	52	55	58	56	56	57
130	62	65	70	68	70	72	55	57	60	58	60	60
131	63	80	94	72	72	72	54	66	86	58	59	60
132	61	67	77	68	71	72	46	52	61	52	56	58
133	64	68	74	66	67	67	49	51	55	51	52	53
134	64	67	71	66	67	67	49	55	72	52	53	53
135	62	66	71	66	66	66	47	51	66	52	52	52
136	63	65	70	65	65	66	48	50	53	49	50	52
137	62	63	65	63	64	64	47	48	50	48	49	49
138	60	62	65	62	63	63	46	48	49	48	48	48
139	61	62	63	62	62	62	47	47	48	47	47	48
140	60	62	63	62	62	62	46	47	48	47	47	48
141	61	63	65	62	62	62	47	48	49	48	48	48
142	60	62	65	62	62	62	46	48	49	47	47	48
143	60	61	64	62	62	62	46	47	49	47	47	47

Long-term 25-year solar variability

As a guide for orbit lifetime planning and debris mitigation purposes, it is often useful to have a 25-year estimate of atmosphere density variability that is driven by solar indices. The following procedure is recommended for producing a consistent, repeatable estimate of long-term 25-year JB2008 thermospheric densities:

1. determine the relative starting point in the solar cycle for the proxies and indices from Tables D1 and D2; the most useful index for this is the F_{81} mean value in Table D1; the start may be at the beginning, rise, maximum, decline, or end of a cycle; for example, to plan a mission with a spacecraft launch in 2012 and to estimate its 25-year lifetime, the assumption would be made that the mission start is approximately at the maximum of cycle 24; an appropriate date in cycle 23 would be selected such as Month 60 where the F_{81} mean value is 223; the F_{81} mean value can be used a generalized indicator of solar cycle phases;

2. form a consecutive set of monthly proxy and index values by concatenating onto Tables D1 and D2 the Month 0 line of the Tables starting in place of Month 124; although solar cycles are often thought of as 11-year cycles, there is actually a range of cycle periods and this method results in an acceptable solar cycle length of 124 months (10 years, 4 months) where the discontinuity between the end of one cycle and the start of another cycle is minimized; the cycle start in the table data set is Month 0, the peak is Month 60, and the cycle end is Month 123 when the table is used to create multiple cycles; it is typical for a solar cycle to have a faster rise to maximum and a slower decline to minimum; the solar cycle minimum is the lowest average value following the peak of the cycle; this method has a slight high flux bias by excluding the lowest solar activity conditions and favors shorter solar cycles; and

Fig. 6. $F_{10.7}$, $S_{10.7}$, $M_{10.7}$, $Y_{10.7}$ (v4.0) daily values for use by the JB2008 model from October 1 to November 30, 2003 during storm conditions.

3. repeat this process for as many months, years, or solar cycles as are needed.

Figure 6 shows the four solar proxies and indices during October 1 to November 30, 2003 in a storm period. The differences in daily variability can easily be seen.

Geomagnetic indices

The geomagnetic indices used in JB2008 incorporate existing as well as expanded empirical modeling formulations compared to previous Jacchia and MSIS-type models. A two-index formulation now captures low, unsettled, and substorm/storm related geomagnetic activity. When the a_p value is 40 and below (unsettled to quiet activity), the a_p value is used. Above that threshold the code assumes that there is a storm/substorm in progress and Dst is used.

a_p index

The a_p index reports the amplitude of planetary geomagnetic activity for a given day (Mayaud, 1980). It is translated from the K_p index, which is derived from geomagnetic field measurements made at several locations around the world. The official a_p values are calculated at the GeoForschungsZentrum Potsdam Adolf-Schmidt-Observatory for Geomagnetism in Germany; for more information, see the website located at (http://www.gfz-potsdam.de/pb2/pb23/GeoMag/niemegk/kp_index/). The daily A_p is obtained by averaging the eight 3-hour values of a_p for each day. The U.S. Air Force Weather Agency also calculates an estimated a_p from a different, smaller set of stations than are used in calculating the official a_p values. The AFWA a_p index values are available through several products issued by NOAA SPWC. Daily Ap and 3-hour

ap indices were used in early orbit analyses and it was determined that the time scales of geomagnetically-induced variability represented by these indices were on the order of a few hours (Moe, 1966; Moe and Nebergall, 1969).

Dst index

The Disturbance Storm Time (Dst) index is an indicator of the strength of the storm-time ring current in the inner magnetosphere. During the main phase of geomagnetic storms, the ring current becomes highly energized and produces a southward-directed magnetic field perturbation at low latitudes on the Earth's surface. This is opposite to the normal northward-directed main field. The quick-look Dst index is calculated hourly and released through the World Data Center (WDC) in Kyoto, Japan (http://swdcwww.kugi.kyoto-u.ac.jp/dst_realtime/index.html) using measurements from four off-equatorial magnetic observatories.

Dst is an 'absolute' index and is reported in units of nT; magnetic observatory data are required for its calculation. Magnetic observatories are specially designed and carefully operated facilities that provide stable-baseline magnetometer data over long periods of time. Typically, an observatory supports the operation of fluxgate, proton-precession, and declination-inclination (theodolite) magnetometer systems. Sensors are situated on stable piers, and along with their acquisition electronics, they are operated in temperature-controlled conditions. Therefore, measurements from the various sensor systems can be combined to produce data that are extremely accurate. Traditionally, four stations have been used for the Dst calculation: Hermanus (HER), South Africa; Kakioka (KAK), Japan; Honolulu (HON), Hawaii; and San Juan (SJG), Puerto Rico. These stations have been continuously operated by national agencies for decades and the data that they produce has high quality. These four stations also provide good longitudinal coverage that is needed to make a global estimation of the average ring-current intensity.

Most magnetic storms begin with sharp decreases (southward-directed negative values) in Dst, called the storm sudden commencement, in response to increased solar wind pressure. Following a southward turning of the interplanetary magnetic field, Dst decreases as ring current energy increases during the storm's main phase. During the recovery phase the ring current energy decreases and Dst increases until the storm's end when the magnetic field perturbation has ceased. In time series traces Dst shows a transition from early to late recovery phases that is characterized by significant changes in the rate of change (slope). This occurs as the distribution of the ring current becomes symmetric in local time. It should be noted that a significant fraction of magnetic storms manifest more complex structuring, including multiple main and partial recovery phases.

Use of Dst as an index for the energy deposited in the thermosphere during magnetic storms is more accurate than the use of the a_p index. This is because Dst has higher temporal resolution with an ability to segregate storm phases with their corresponding magnitudes. On the other hand, the 3-hour a_p index is an indicator of general magnetic activity over the Earth and responds primarily to currents flowing in the ionosphere and only secondarily to magnetospheric variations. The a_p index is derived from measurements by observatories at high latitudes that can be blind to energy input during large storms and it can underestimate the effects of storms on

the thermosphere.

During storm periods the thermosphere acts as a driven-but-dissipative system whose dynamics are represented by a differential equation and where the changes in exospheric temperature change due to storm effects can be expressed as a function of Dst. To determine the effects on exospheric temperature, and thereby the thermospheric density distribution at any time in a storm, it is necessary to integrate the differential equation taking into account the change in exospheric temperature, dTc, while starting at the storm commencement and proceeding throughout the entire storm period. An algorithm for determining the storm events was developed (Bowman *et al.,* 2008a) that locates the temporal start, minimum, recovery slope change, and final end of the storm as reflected in the Dst index. The algorithm can incorporate the changes due to multiple or complex storms. The a_p, Dst, and dTc values used to drive JB2008 thermospheric densities that are a result of geomagnetic activity are updated hourly and provided at the JB2008 website accessible through the JB2008 menu link at https://spacewx.com.
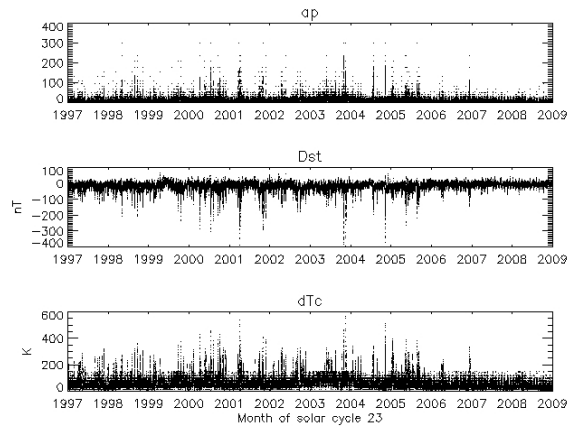
Fig. 7. The a_p, Dst, and dTc geomagnetic, ring current, and delta temperature indices for use by the JB2008 model in solar cycle 23.

a_p geomagnetic variability and Dst storm and substorm variability

Low, moderate or high values for a_p can occur at any time in the solar cycle. Table E shows the a_p high-latitude planetary geomagnetic index, the Dst ring current index, and the change in exospheric temperature dTc for an example storm on November 20-21, 2003 over the course of 48 hours. Figures 7 and 8 show the a_p, Dst, and dTc indices for solar cycle 23 and for a storm period of November 19–22, 2003.

In short-term periods, higher values than those given in Table E have been measured, e.g., a_p= 400 for 3 hours. However, empirical atmosphere density models are not developed for such high index values and their use will lead to large and unknown errors. When JB2008 is run for long periods without consideration of storms, e.g., using Tables D1 and D2 or the 25-year prediction method, a suitable low level constant a_p can be used such as the historical long-term mean value, a_p = 12. The long-term historical mean value of Dst = -15 and the historical long-term mean value of dTc = 58.
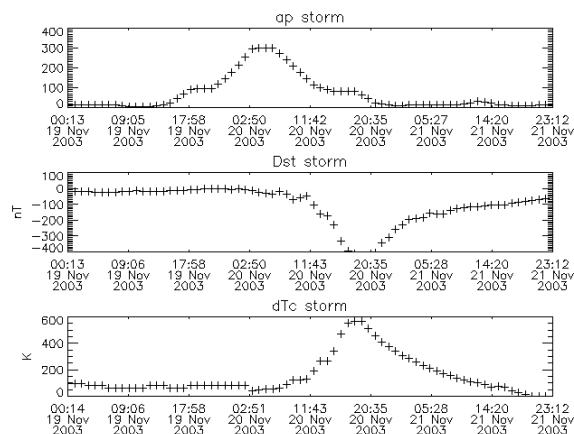

Fig. 8. The a_p, Dst, and dTc geomagnetic, ring current, and delta temperature indices for use by the JB2008 model in a storm period between November 19–22, 2003.

Outstanding issues

There are several outstanding issues related to JB2008 solar indices' improvements. First, there is 1–2% error introduced into the indices' relative yearly variability resulting from the mixed use of 1 AU and observed values. The $F_{10.7}$ and 0.1–0.8 nm GOES X-rays are used as observed values, i.e., uncorrected to 1 AU. The X-rays are used to form half of the $Y_{10.7}$ index. The Lyman-α used to derive $Y_{10.7}$, $S_{10.7}$, and Mg II cwr used to derive $M_{10.7}$ are corrected to 1 AU. While these errors do not dominate the uncertainty in modeling thermospheric densities, a common approach such as 1 AU uncorrected, observed values would be appropriate for all proxies and indices and this would reduce potential error in the density modeling.

Second, the calibration of SOHO/SEM 26–34 nm broadband data with spectrally integrated irradiance data from TIMED/SEE is important to complete. The resolution of this comparison would allow other new spectral datasets such as SDO/EVE to be converted to an $S_{10.7}$ index as a backup dataset.

Third, the solar cycle 23 minimum values for the solar indices should be reexamined in comparison with the cycle 22 minimum values. Fitting algorithm artifacts may not model well the transition into the start of solar cycle 24.

Conclusions

Four solar irradiance proxies and indices are described that are used in the JB2008 thermospheric density model. Three of them, $F_{10.7}$, $S_{10.7}$, $M_{10.7}$, were previously discussed in literature describing the JB2006 model and the fourth, $Y_{10.7}$, is similar to a previously described $XL_{10.7}$ from the JB2006 discussion and is fully described here. Use of these solar indices in the JB2008 model produces significant improvements in empirical thermospheric density modeling. JB2008 provides standard deviations of approximately 9–10% at 400 km, which is a significant decrease from 16% previously obtained using the Jacchia 70 model (Bowman *et al.*, 2008a).

The experience in developing the preceding model, JB2006, showed that different solar atmosphere temperature regions and features create specific solar wavelengths and these map into separate levels of unit optical depth in the thermosphere. In JB2006 three solar indices were derived to represent this mapping of solar irradiance sources to thermospheric optical depths. JB2008 further extended this methodology to include an additional solar temperature region (the hot corona) and an additional thermospheric layer, i.e., the 85-100 km mesopause to lower thermosphere. The $Y_{10.7}$ index is used to capture this mapping.

The characteristics of each solar proxy and index are tabulated in the context of their utility for operational uses. These solar proxies and indices are compliant with the ISO International Standard 21348 for determining solar irradiances. Reference values of the solar indices and proxies for short-term, intermediate-term, solar cycle, and 25-year periods are provided for users who want reference values for planning and tests. The reference values come from examples in solar cycle 23.

The geomagnetic indices for JB2008 are used in a two-index formulation that captures both low/unsettled activity and substorms/storms. When a_p is 40 and below (unsettled to quiet activity), the a_p value is used. Above that level, the code assumes that there is a storm/substorm in progress and Dst is used. The storm effects change the rate of exospheric temperature change, dTc, which affects satellite orbits. Reference values for a_p, Dst, and dTc are provided using an example storm of November

20-21, 2003 for users who want reference values for planning and tests.

Table E. Example values for a_p, Dst, and dTc storm variability

Time [hrs]	a_p	Dst	dTc
0	4	-004	85
1	4	-006	85
2	4	-005	85
3	22	-007	85
4	22	-015	38
5	22	-026	50
6	94	-032	56
7	94	-034	56
8	94	-017	63
9	94	-038	86
10	94	-068	122
11	94	-058	126
12	179	-049	130
13	179	-102	193
14	179	-162	266
15	300	-171	268
16	300	-229	339
17	300	-329	469
18	300	-396	551
19	300	-413	563
20	300	-422	564
21	207	-422	509
22	207	-405	457
23	207	-343	412
24	111	-309	372
25	111	-256	339
26	111	-230	309
27	80	-194	283
28	80	-191	259
29	80	-185	235
30	80	-156	214
31	80	-162	193
32	80	-162	172
33	22	-141	154
34	22	-130	137
35	22	-122	121
36	7	-118	106
37	7	-117	103
38	7	-110	86
39	15	-104	71
40	15	-105	72
41	15	-104	70
42	12	-092	40
43	12	-086	25
44	12	-083	17
45	12	-076	0
46	12	-069	0
47	12	-063	0

Access to JB2008 historical, current epoch, and forecast indices

The indices described here for input into the JB2008 model, as well as the model Fortran source code, are provided by Space Environment Technologies at the JB2008 menu link on the website https://spacewx.com. The Solar Irradiance Platform (SIP) provides historical, current epoch, and forecast daily JB2008 indices and proxies up-dated hourly with daily time granularity, as well as full spectral irradiances and real-

time solar activity monitoring for satellite and communication system operations. SIP can be downloaded at the https://spacewx.com SIP menu link.

References

Banks, P. and G. Kockarts, *Aeronomy*, Academic Press, New York, 1973.

Bouwer, S.D., MgII c/w Ratio Data Processing for SET Operations, *SET_TR2008-001*, Space Environment Technologies Technical Report, July 2008.

Bowman, B.R., W.K. Tobiska, F.A. Marcos, C.Y. Huang, C.S. Lin, W.J. Burke, A New Empirical Thermospheric Density Model JB2008 Using New Solar and Geomagnetic Indices, AIAA/AAS Astrodynamics Specialist Conference, AIAA 2008-6438, 2008a.

Bowman, B.R., W.K. Tobiska, M.J. Kendra, The thermospheric semiannual density response to solar EUV heating, *J. Atm. Solar-Terr. Phys.*, 2008b.

Bowman, B.R., W.K. Tobiska, F.A. Marcos, and C. Valladares, The JB2006 empirical thermospheric density model, *J. Atm. Solar-Terr. Phys.*, **70**, 774-793, 2008c.

COSPAR International Reference Atmosphere 1972, compiled by the COSPAR Working Group IV, North-Holland Publishing Co., Amsterdam, 1972.

Covington, A.E., Solar noise observations on 10.7 centimeters, *Proc. of the I.R.E.,* **36,** 454, 1948.

DeLand, M.T. and R.P. Cebula, Comparisons of the Mg II index products from the NOAA-9 and NOAA-11 SBUV/2 instruments, *Solar Phys.,* **152**, 61-68, 1994.

Cebula, R.P., and M.T. DeLand, Comparisons of the NOAA-11 SBUV/2, UARS SOLSTICE, and UARS SUSIM Mg II solar activity proxy indexes, *Solar Phys.,* **177**, 117-132, 1998.

Heath, D.F. and B.M. Schlesinger, The Mg 280-nm doublet as a monitor of changes in solar ultraviolet irradiance, *J. Geophys. Res.,* **91,** 8672-8682, 1986.

ISO 21348, Space Environment (natural and artificial) – Process for determining solar irradiances, International Standards Organization (ISO), Geneva, 2007.

Jacchia, L.G., Static diffusion models of the upper atmosphere with empirical temperature profiles, *Smithson. Contr. Astrophys.,* **8,** 215, 1965.

Jacchia, L.G., Revised static models of the thermosphere and exosphere with empirical temperature profiles, *Smithson. Astrophys. Special Report 332*, 1971.

Judge, D.L., H.S. Ogawa, D.R. McMullin, P. Gangopadhyay, and J.M. Pap, The SOHO CELIAS/SEM EUV Database from SC23 Minimum to the Present, *Adv. Space Res.,* **29** (12), 1963, 2001.

Mayaud, P.N., Derivation, Meaning, and Use of Geomagnetic Indices, *Geophysical Monograph 22,* American Geophysical Union, Washington, DC, 1980.

Marcos, F.A., B.R. Bowman, and R.E. Sheehan, Accuracy of Earth's thermospheric neutral density models, AIAA 2006-6167, *AIAA/AAS Astrodynamics Specialist Conference*, Keystone, CO, August, 2006.

Moe, K., Absolute atmospheric densities determined from the spin and orbital decays of Explorer VI, *Planet. Space Sci.,* **14**, 1065-1075, 1966.

Moe, K. and D. Nebergall, Variation of geomagnetic disturbance with latitude, *J. Geophys. Res.,* **74**, 1305-1307, 1969.

Paetzold, H.-K., *COSPAR Space Research*, Nice, 1960.

Priester, W., *Naturwissenschaften*, **46**, 197, 1959.

Schmidtke, G., *Geophys. Res. Lett.,* 3, 573, 1976.

Tapping, K.F. and B. DeTracey, The origin of the 10.7 cm flux, *Solar Phys.,* **127** (2), 321-332, 1990.

Tobiska, W.K., *A Solar Extreme Ultraviolet Flux Model,* Ph.D. Thesis, Department of Aerospace Engineering, University of Colorado, 1988.

Tobiska, W.K. and S.D. Bouwer, Solar flare evolution model for operational users, *2005 Ionospheric Effects Symposium,* ed. J.M. Goodman, JMG Associates, 76, 2005.

Tobiska, W.K., S.D. Bouwer, B.R. Bowman, The development of new solar indices for use in thermospheric density modeling, *J. Atm. Solar-Terr. Phys.,* **70,** 803–819, 2008.

Vernazza, J.E., Avrett, E.H., Loeser, R., Structure of the solar chromosphere: II. The underlying photosphere and temperature-minimum region, *Astrophysical Journal Supplement Series* **30**, 1–60, 1976.

Vernazza, J.E., Avrett, E.H., Loeser, R., Structure of the solar chromosphere: III. Models of the EUV brightness components of the quiet Sun, *Astrophysical Journal Supplement Series* **45**, 635–725, 1981.

Viereck, R., L. Puga, D. McMullin, D. Judge, M. Weber, W.K. Tobiska, The Mg II Index: A Proxy for Solar EUV, *Geophys. Res. Lett.,* **28** (7), 1342, 2001.